Journal of Power Electronics (2021) 21:647–659
https://doi.org/10.1007/s43236-020-00201-9

ORIGINAL ARTICLE

Fault-tolerant analysis of two boost inverters for open-end winding induction motor drives

Chunjie Li[1] · Guifeng Wang[1] · Hongmei Li[1] · Fei Li[1] · Zhenglong Xia[1] · Zhan Liu[1]

Received: 17 March 2020 / Revised: 9 December 2020 / Accepted: 10 December 2020 / Published online: 10 February 2021

Abstract
An open-end winding induction motor drive system fed by two boost inverters with fault-tolerant capability is presented to improve the reliability and safety of the drive system. The boost inverters consist of an impedance-source network and a two-level inverter. It can realize the boost/buck function. An analysis of its fault-tolerance is presented in detail. Short circuits and open circuits are commonly considered as the two main types of faults. Therefore, the fault types of the dual boost inverters are analyzed and diagnosed. Then, two different fault-tolerant schemes are presented. The presented fault-tolerant inverters are restructured through the power switch itself. In addition, different SVPWM methods are addressed. A simulation model and an experimental platform are constructed. Simulation and experimental results verify the fault tolerance of the drive system.

Keywords Dual-boost inverters · Fault tolerance · Impedance-source network · Open-end winding induction motor

1 Introduction

With the rapid development of power electronics, PWM inverter-fed induction motor drives have been widely accepted in industrial applications, such as aircraft power systems and electric vehicle (EV) drive systems [1]. After the failure of a motor drive system, the motor runs asymmetrically, and the output torque pulsates, resulting in large mechanical noise. This can result in system performance decline or even system failure. Therefore, fault-tolerant control capability has become a very prominent problem for drive systems with high reliability. The voltage-source inverter is taken as an important component for drive systems, where the failure probability directly affects the operation of the motor drive system. The most important faults for voltage-fed inverters are either main-side diode or transistor converter faults [2]. References [3, 4] analyze the fault percentages of the components in converters. However, relative results show that power switches and electrolytic capacitors are usually regarded as fragile and easy to break down due to short-circuit faults. Meanwhile, the stator windings in motor drive systems are also considered easy to produce open circuits. Both types of faults mentioned above lead to a shutting down of the whole drive system. The importance of the reliability of a drive system cannot be ignored.

In recent years, novel multilevel inverter topologies have appeared and been applied in open-winding motor drive systems [5–15]. These open-winding motors are typical induction motors with a modification to provide six terminals of the three stator windings. In other words, the internal neutral point connection is removed. For these kinds of the motor drives, several multilevel inverter topologies have been proposed and investigated. One of the most important topologies is the dual-inverter configuration. The dual-inverter configuration was first presented in 1993 [16]. However, deep research has only started recently because of many advantages, such as higher AC voltage levels, reduced harmonic distortion, lower electromagnetic interference, and especially strong fault-tolerant capability [5]. Depending on whether the power supply is shared or not, dual inverters can be categorized into two types, single power supply [9, 10] and double separate power supplies [13–15]. When compared with single power supply drive systems, dual-inverter drive systems have one more power supply. Although its cost is higher, and both the power density and power utilization are lower [9], there is no zero sequence current and inverters can obtain an output of more levels. Many studies have addressed the topologies and the modulation methods of traditional dual-inverters for open-end

✉ Guifeng Wang
wgfmy@163.com

[1] Department of Electrical Engineering and Automation, Jiangsu Normal University, Xuzhou, China

winding induction motors (IM) [5, 9–20]. In addition, fault-tolerant control has been analyzed in [5, 8, 21]. Reference [5] achieves fault-tolerance through three traditional three-phase inverters, which are buck converters and cannot allow a shoot-through state. All of the topologies mentioned suffer from problems. Table 1 presents a comparison of the above converter topologies for open-end winding induction motor drives. From Table 1, it can be seen that traditional voltage-source inverter-fed drive system has buck functionality and low reliability.

For EVs powered by batteries, a large current discharge can cause a terminal voltage drop of the battery pack. This leads to a mechanical power reduction, which affects the dynamic performance of the EVs. In addition, when an EV runs at high speeds, the limited stator voltage output by a traditional inverter cannot satisfy it. However, impedance-source inverters [22] can resolve these problems, which can keep the DC bus voltage constant because of its boost capability [23]. Due to the insertion of an impedance-source network, the AC output voltage of the impedance-source inverter is not affected by terminal voltage drops of the battery. Instead, it is determined by the boost coefficient B of the impedance-source network and the PWM modulation ratio M of the inverter. The output DC bus voltage of the impedance-source network is only related to the input voltage and the boost coefficient. However, it can be seen from Table 1, that when compared with the traditional boost inverter in [10], it has higher boost capability and allows for the shoot-through state as well as single-stage conversion [24].

In this paper, a new driving topology configuration is presented and addressed for introducing an impedance-source network to a dual-inverter-fed drive system, which can improve the reliability and achieve boost/buck function and fault-tolerance simultaneously. In addition, an analysis of its fault tolerance is fully discussed and addressed. SVPWM methods for the different fault-tolerant inverter structures are also presented. A simulation model and an experiment platform are constructed. Simulation and experimental results verify the fault-tolerance of the drive system.

2 Two boost inverters for open-end winding induction motor drives

2.1 Topology analysis

The topology is shown in Fig. 1, which is composed of two power supplies, two three-phase impedance-source inverters (boost inverters), and an open-end winding induction motor (IM). There exists a shoot-through state because of the impedance-source network, which is different from three-phase traditional inverters. The principle and the working states of the impedance-source inverter can be found in [22–25]. Thus, they are not addressed in detail in this paper.

2.2 Quantitative analysis

The open-winding induction motor drive system in this paper adopts two separate power supplies. Suppose that the induction motor winding and a boost inverter are regarded as a node in Fig. 1. Then, according to Kirchhoff's current law, the sum of the currents flowing into the node is zero. In other words, the current of the other three-phase boost inverter is $i_A + i_B + i_C = 0$. Therefore, there is no zero sequence voltage or current in the open-winding motor system powered by two boost power supplies.

In Fig. 1, the load phase–voltage can be obtained as follows:

$$\begin{cases} U_{A1A2} = U_{A1O} - U_{A2O'} + U_{OO'} \\ U_{B1B2} = U_{B1O} - U_{B2O'} + U_{OO'} \\ U_{C1C2} = U_{C1O} - U_{C2O'} + U_{OO'} \end{cases}. \tag{1}$$

The induction motor winding and boost inverter 1 are regarded as a node. Then, from Kirchhoff's current law, the three-phase stator currents for boost inverter 2 can be derived as:

$$i_A + i_B + i_C = 0. \tag{2}$$

Three-phase stator voltage equation is as follows:

$$\begin{cases} U_{A1A2} = Ri_A + p\psi_A \\ U_{B1B2} = Ri_B + p\psi_B \\ U_{C1C2} = Ri_C + p\psi_C \end{cases}, \tag{3}$$

where ψ_A, ψ_B, ψ_C denote the magnetic flux of the stator; and R describes the internal resistance of the stator.

The magnetic flux equation is presented as:

$$\begin{cases} \psi_A = L_{ss}i_A - M_s i_B - M_s i_C - M_{sr}\cos\ \theta i_a + M_{sr}\cos\ (\theta + 120°)i_b \\ \qquad + M_{sr}\cos\ (\theta - 120°)i_c \\ \psi_B = L_{ss}i_B - M_s i_A - M_s i_C - M_{sr}\cos\ \theta i_b + M_{sr}\cos\ (\theta + 120°)i_c \\ \qquad + M_{sr}\cos\ (\theta - 120°)i_a \\ \psi_C = L_{ss}i_C - M_s i_A - M_s i_B - M_{sr}\cos\ \theta i_c + M_{sr}\cos\ (\theta + 120°)i_a \\ \qquad + M_{sr}\cos\ (\theta - 120°)i_b \\ \psi_a = L_{rr}i_a - M_r i_b - M_r i_c - M_{sr}\cos\ \theta i_A + M_{sr}\cos\ (\theta + 120°)i_C \\ \qquad + M_{sr}\cos\ (\theta - 120°)i_b \\ \psi_b = L_{rr}i_b - M_r i_a - M_r i_c - M_{sr}\cos\ \theta i_B + M_{sr}\cos\ (\theta + 120°)i_A \\ \qquad + M_{sr}\cos\ (\theta - 120°)i_C \\ \psi_c = L_{rr}i_c - M_r i_a - M_r i_b - M_{sr}\cos\ \theta i_C + M_{sr}\cos\ (\theta + 120°)i_B \\ \qquad + M_{sr}\cos\ (\theta - 120°)i_A \end{cases}, \tag{4}$$

Table 1 Comparison of converter topologies for open-end winding induction motor drives

Topologies	Structure characteristics	Buck/boost function	Reliability	Modulation methods
New 3yVSC modular multilevel inverter topology [5]	Three two-level three-phase voltage source converters, more power devices	Buck	Low	PD-PWM and PSM-PWM
Dual two-level inverter topology for three-level/four-level inversion with equal or unequal dc-link voltages [6, 9, 11, 17–20]	Two two-level three-phase voltage-source converters, more power devices	Buck	Low	CMV elimination PWM, SIM and TIM PWM methods, an improvised scheme (center spaced PWM (CSPWM) technique + phase clamped PWM)
Nine-level asymmetrical multilevel inverter [10]	Boost converter + 6 H-bridge inverters, most power devices, more voltage levels, two-stage conversion	Boost/buck	Low	Nearest level control (NLC) modulation strategy
Two two-level inverters in cascade at one end and a single two-level inverter at the other end [12]	Three two-level three-phase voltage-source converters, more power devices	Buck	Low	Space-vector pulse width modulation (SVPWM)
Dual-inverter system composed of a traditional inverter and a floating bridge [13, 21]	Two two-level three-phase voltage-source converters + an extra electrolytic capacitor	Buck	Low	RFO control scheme and SVM modulation
Open-end winding four-level five-phase drive [14]	Two five-phase voltage-source converters	Buck	Low	Two-level-shifted carrier-based PWM methods
Nine-level power converter topology [15]	Two conventional three-phase two-level voltage-source inverters powered by isolated dc sources and six floating-capacitor-connected *H*-bridges, more voltage levels, most power devices	Buck	Low	SVPWM
The presented topology	Impedance-source network + two three-phase voltage-source converters, single-stage conversion, higher boost, allows for shoot-through state	Buck/boost	High	SVPWM

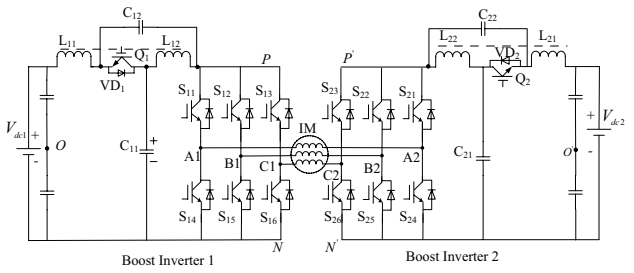

Fig. 1 Two boost inverters for an open-end winding induction motor drive

where ψ_a, ψ_b, ψ_c denote the magnetic flux of the rotor; L_{ss} indicates the self-inductance of the stator; L_{rr} is the self-inductance of the rotor; M_s and M_r represent the mutual inductance of the stator and rotor; and M_{sr} denotes the mutual inductance between the stator and the rotor.

From (2–4), the voltage equation can be derived as follows:

$$U_{A1A2} + U_{B1B2} + U_{C1C2} = 0. \tag{5}$$

From (1) and (5), the common mode voltage $U_{OO'}$ can be obtained as:

$$U_{OO'} = \left(U_{A1O} + U_{B1O} + U_{C1O} - U_{A2O'} - U_{B2O'} - U_{C2O'}\right)/3. \tag{6}$$

From (6), it can be found that there is a common mode voltage of an open-winding induction motor fed by double-boost inverters. The existence of this common mode voltage can bring a lot of adverse effects on the operation of an induction motor [6], such as zero sequence current (common mode currents) that greatly reduces the current quality, shaft current that can make the motor bearings burn, and motor vibration. Therefore, the common mode voltage should be suppressed [20].

2.3 SVPWM method

A space voltage vector diagram of double-boost inverters with the same DC-voltage value is shown in Fig. 2, which consists of the switching states for the two three-phase boost inverters. Through an analysis of all the space voltage vectors in Fig. 2, it can be seen that the space voltage vectors of the regular hexagon HJLNQS do not generate common mode voltage [20, 26]. Thus, a reasonable selection of the space voltage vectors can eliminate common mode voltage.

3 Analysis of fault-tolerant schemes

To solve the short circuits of power switches, and the open circuits of power switches and motor windings, it is necessary to reconstruct the topology. The control method changes

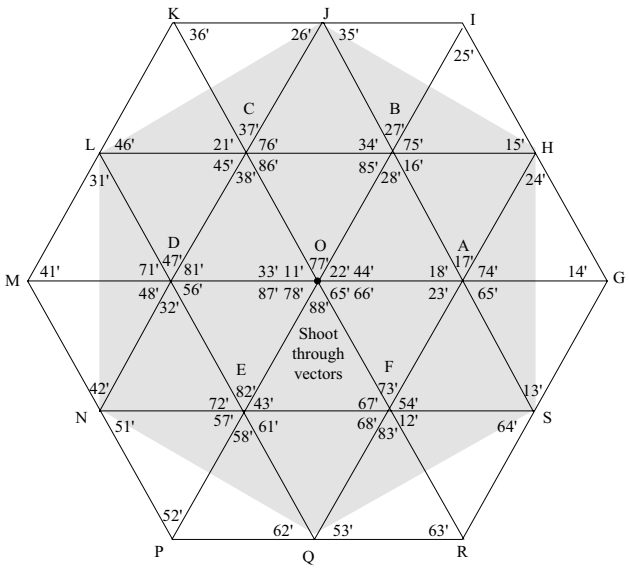

Fig. 2 Space voltage vector diagram of two three-phase boost inverters

as the topology changes. Therefore, the space voltage vectors of the post-fault topology are analyzed.

3.1 Fault analysis

The open-winding induction motor is driven by a power electronic converter. When compared with the motor structure itself, the power electronic converter is more prone to failure. There are two main kinds of power switch faults. The first type is the short-circuit fault, which is caused by the reverse breakdown of switches or the destruction of the insulation layer. The second type is the open-circuit fault, which is caused by the drive circuit of the power switch itself.

Since the probability of more than two power switches or windings failing at the same time is very small, only a single switch fault is considered in this paper.

3.2 Short-circuit fault diagnosis of power switches

To determine which switch is short, the switch voltage drop should be detected. If the average voltage is zero within a switching period, there is a short-circuit fault. Then, the switch whose voltage drop is zero is short.

Suppose that a short-circuit fault of the switch S_{11} occurs as shown in Fig. 3. The node $A1$ and the positive electrode of the DC bus voltage are isoelectric points, and the voltage drop of the switch S_{11} is zero. The phase-A winding cannot be driven. The motor drive system cannot work normally.

According to a comparison of IGBT short-circuit fault diagnostic methods in [27], the average current Park's vector approach is selected since it has high reliability and is easy

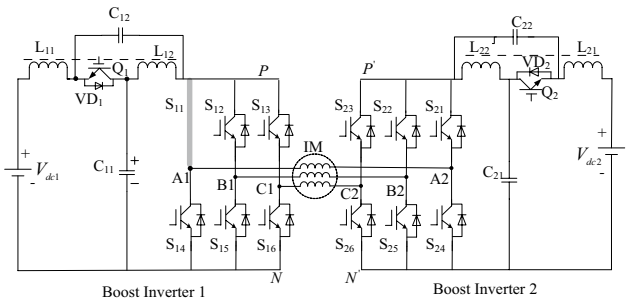

Fig. 3 Topology with a short-circuit fault of the power switch S_{11}

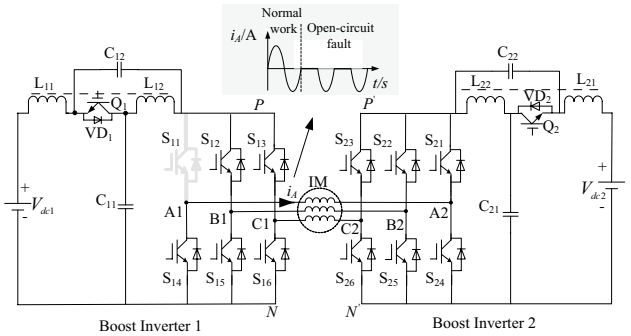

Fig. 4 Open-circuit fault of the power switch S_{11}

to combine with motor drive control systems. The occurrence of short-circuit faults of controlled power switches is characterized by the average motor supply current Park's vectors modulus, different from zero and greater than the ones corresponding to the open-circuit faults of controlled power switches. Then, the modulus and the threshold value are used to make a comparison to identify an open fault or a short-circuit fault. Then, the fault location is determined by combining the phase angle. Detailed implementation on this procedure can be found in [28].

3.3 Open-circuit fault diagnosis of power switches

To diagnose an open-circuit fault, the winding current and the switch voltage drop need to be tested. If the average value of the winding current is zero in half of a power cycle, the circuit loop is broken. If one switch voltage drop is high level, and not zero in a switching period, the switch is broken.

Suppose that an open-circuit fault of the switch S_{11} appears as shown in Fig. 4. The winding current of phase-A is negative semi-sine in a line period. The drive system cannot work normally. Next, a method to diagnose a fault is presented.

In addition to the above average current Park's vector approach based on current fault diagnostics, there are many detection methods based on voltage fault diagnostics [27]. Among them, the lower switch voltage-sensing method with a shorter diagnostic time and a simpler algorithm can diagnose open faults of power switches [4]. However, in the two three-phase inverters, more voltage sensors are used. Thus, the average current Park's vector approach is adopted in the drive system.

3.4 Fault-tolerant reconstruction

When a power switch produces fault, the other relative switches are controlled to make the fault bridge arm inoperative, and the other bridge arms drive the motor. Taking the fault of the switch S_{11} as an example, the fault-tolerant reconstruction is expounded. There are two fault-tolerant schemes.

The first fault-tolerant scheme is described as follows. When an open-circuit fault of the switch S_{11} is detected, the drive signal of the switch S_{11} is blocked, and the drive signals of the switches S_{14}, S_{21} and S_{24} are also blocked. Then, the phase-A winding does not participate in the drive system. The drive system can work through the remaining two-phase boost inverter.

After detecting a short-circuit fault of the switch S_{11}, the drive signals of the switches S_{14}, S_{21} and S_{24} are blocked. Then, the phase-A winding becomes inoperable. The drive system can work through the remaining two-phase inverter. However, the fault-tolerant topology can be improved.

To ensure symmetry of the two-phase inverters, it is necessary to cut off the drive signals of the four switches in the fault phase, and the fault-phase winding does not participate in the drive system. The induction motor is in the remaining two-phase running state. The remaining two-phase post-fault currents are equal in magnitude, with a phase difference of 180°. In addition, this structure cannot make the motor produce a circular rotating magnetic field. To realize fault-tolerant control, the points N and N' are connected and the points P and P' are connected. Therefore, the fault-tolerant circuit structure shares the same DC power supply [26].

The fault-tolerant topology is presented in Fig. 5. Figure 5a presents the two-phase fault-tolerant topology when there is a short-circuit fault of the switch S_{11}. The body-diode in the switch S_{21} turns on when withstanding forward voltage. At this moment, the phase-A winding is at the free-wheeling state through the switch S_{11} and the body-diode in the switch S_{21}. Figure 5b shows the two-phase fault-tolerant topology when there is an open-circuit fault of the power switch S_{11}. This fault-tolerant structure is also suitable for an open fault of the one-phase motor winding. From Fig. 5, it can be seen that the two fault-tolerant topologies share a DC power supply.

For the second fault-tolerant scheme, the drive system is in three-phase operation. Taking a fault of the switch S_{11}

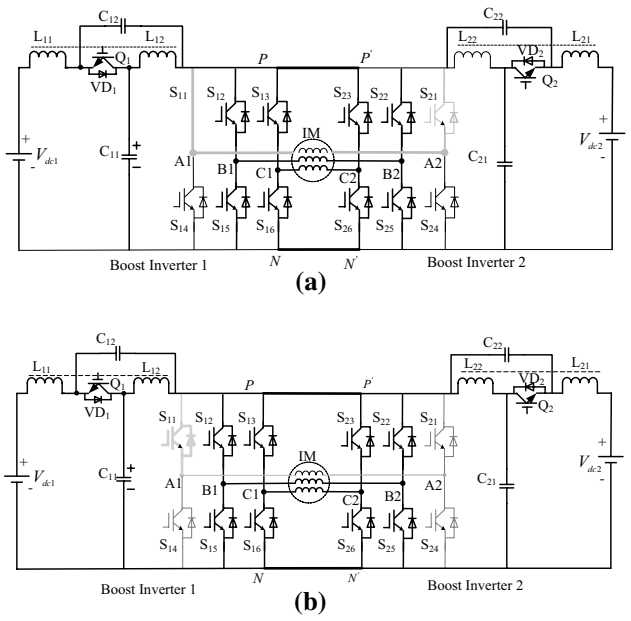

Fig. 5 Two-phase fault-tolerant topology: **a** fault-tolerant topology of a short-circuit fault; **b** fault-tolerant topology of an open-circuit fault

as an example, the fault-tolerant topology structure can be described as follows.

When there is an open-circuit fault of the upper switch S_{11}, the upper switches S_{12} and S_{13} in the faulty inverter keep turning off, while the lower switches S_{14}, S_{15} and S_{16} keep turning on. The fault-tolerant topology is presented in Fig. 6. From Fig. 6, it can be found that the open-winding induction motor becomes a star-connected general-motor.

When there is a short-circuit fault of the switch S_{14} in boost inverter 1, the switches S_{15} and S_{16} keep turning on. Then, the end of three-phase winding connecting to boost inverter 1 can be connected to a node through the switches S_{14}, S_{15} and S_{16}. In other words, the winding is connected in a star configuration. Then, the motor operates symmetrically in three phases using one three-phase boost inverter. From the above analysis, it can be found that when an open-circuit fault or a short-circuit fault of the power switch occurs, the topology can be reconstituted as a three-phase fault-tolerant structure.

The second fault-tolerant scheme is also suitable for faults of multiple upper switches or lower switches in one three-phase inverter. The topology structure becomes simple and reduces the switching losses. In addition, DC-link of the two inverters cannot be connected together.

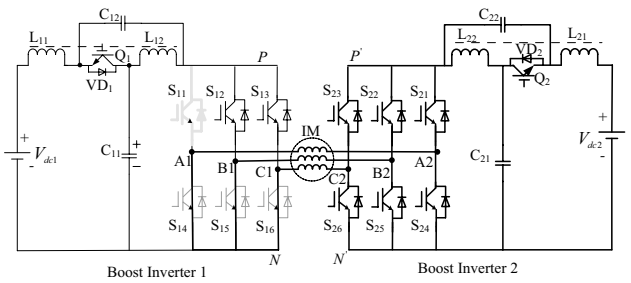

Fig. 6 Three-phase fault-tolerant topology

3.5 SVPWM for the fault-tolerant topology

When a switch S_{11} fault appears, removing the turn-on states of the switch S_{11}, the diagram of the remaining space voltage vectors is presented in Fig. 7. From Fig. 7, it can be seen that there are 13 remaining non-zero voltage vectors and 1 zero voltage vector. The remaining active voltage vectors corresponding to the switch states are still redundant. If all of the remaining voltage vectors are used for modulation, the switching times and the switching times of the two inverters are different due to the different voltage vectors. Therefore, the two inverters run asymmetrically. This is unfavorable in terms of controlling the motor. Choosing appropriate voltage vectors is needed. The space voltage vector diagram for the two-phase fault-tolerant topology (the first fault-tolerant scheme) shown in Fig. 5 and the second fault-tolerant scheme shown in Fig. 6 can be presented in Fig. 8.

It can be seen from Fig. 8 that the regular hexagon ABCDEF, which is composed of selected space voltage vectors, can be used to realize the fault-tolerance algorithm and generate a circular rotating magnetic field. The switching states in each of the sectors of the above two fault-tolerant control schemes are shown in Table 2. These values correspond to Figs. 7 and 8.

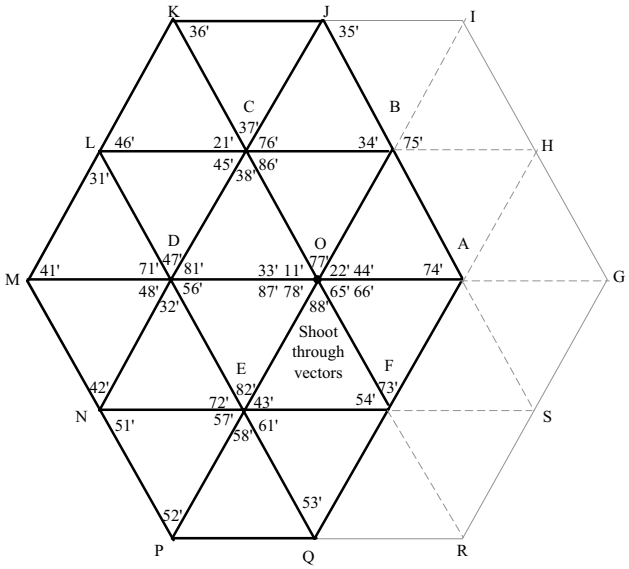

Fig. 7 Post-fault space voltage vector diagram

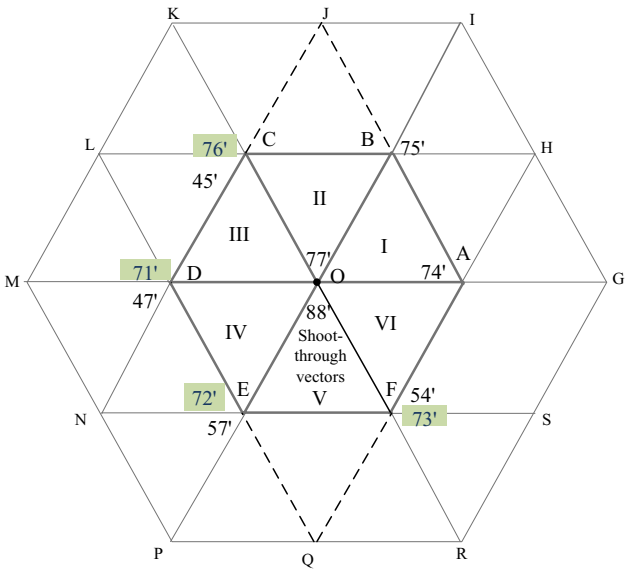

Fig. 8 Space voltage vector diagram for the second fault-tolerant topology

3.6 Drive signal implementation

Figure 9 shows the drive signals of the power switches for the fault-tolerant topology. Figure 9a presents the drive signals for the two-phase fault-tolerant topology. Inserting the shoot-through vectors cannot affect the active vectors. Figure 9b gives the drive signals for the three-phase fault-tolerant topology.

4 Simulation

MATLAB Simulink simulation software is adopted in this paper. A simulation model of an open-end winding induction motor drive system is built and the simulation parameters are presented in Table 3.

From Fig. 5, it can be derived that both the reconstruction topology for a short-circuit fault and the fault-tolerant topology for an open-circuit fault can be regarded as two-phase H-bridge fault-tolerant inverters. Taking an open-circuit fault as an example, the related simulation results are given.

Simulation waveforms are presented in Fig. 10 when the motor speed is 80 rad/s, the load torque is 10 Nm, and the input voltage is 250 V. Before 3 s, the asynchronous motor is under normal operation. Figure 10a shows a waveform of the DC-link bus voltage, which is composed of high-frequency rectangular wave with a constant amplitude that is higher than the input voltage. The amplitude of the three-phase stator winding currents is equal, and the current waveforms are sinusoidal, as shown in Fig. 10b. A speed waveform and a torque waveform are shown in Fig. 10c, d, respectively. From Fig. 10c, it can be seen that the real speed can still track the reference speed well after fault tolerance. In addition, both of the speed ripples are very small. From Fig. 10d, it can be found that the torque ripple coefficient is about 5% under the normal condition. Under the fault-tolerant condition, the two-phase restructured topology drives a two-phase motor. The relative torque ripple is about 10–15%, which is slightly larger than that under normal conditions. Through the above analysis, it may be accepted in the traffic industry since it does not require a precise and accurate torque. This scheme is especially suitable for open circuit of one-phase motor winding.

Simulation waveforms of the three-phase fault-tolerant topology are shown in Fig. 11 when the motor speed is 80 rad/s, and the load torque is 5 Nm, when only one three-phase two-level boost inverter works, and the open-end winding motor becomes a common motor with a wye connection. Figure 11a presents three-phase stator winding currents. The phase difference of the three-phase current is still 120°. The output speed and the torque are basically unchanged, as shown in Fig. 11b, c. It can be seen that the torque ripple is about 5% under the fault-tolerant condition. In addition, the real speed can track the reference speed well. Figure 11d shows the total harmonic distortion (THD) of the one-phase stator winding current. The THD value is about 3.07%. From Fig. 11, it can be found that the second fault-tolerant scheme is verified.

The stator winding currents and the total harmonic distortion (THD) under the faulty condition and under the fault-tolerant condition are presented in Fig. 12. Figure 12a shows the stator winding currents under the two cases of the open-fault mode and the fault-tolerant operation mode. Figure 12b, c presents the THD of the stator winding current, respectively. From Fig. 12b, c, it can be

Table 2 Switching states of each sector for two fault-tolerant schemes

Fault-tolerant schemes	Sectors					
	I	II	III	IV	V	VI
1	74′	45′	47′	47′	54′	54′
	75′	75′	45′	57′	57′	74′
2	74′	76′	76′	72′	72′	74′
	75′	75′	71′	71′	73′	73′

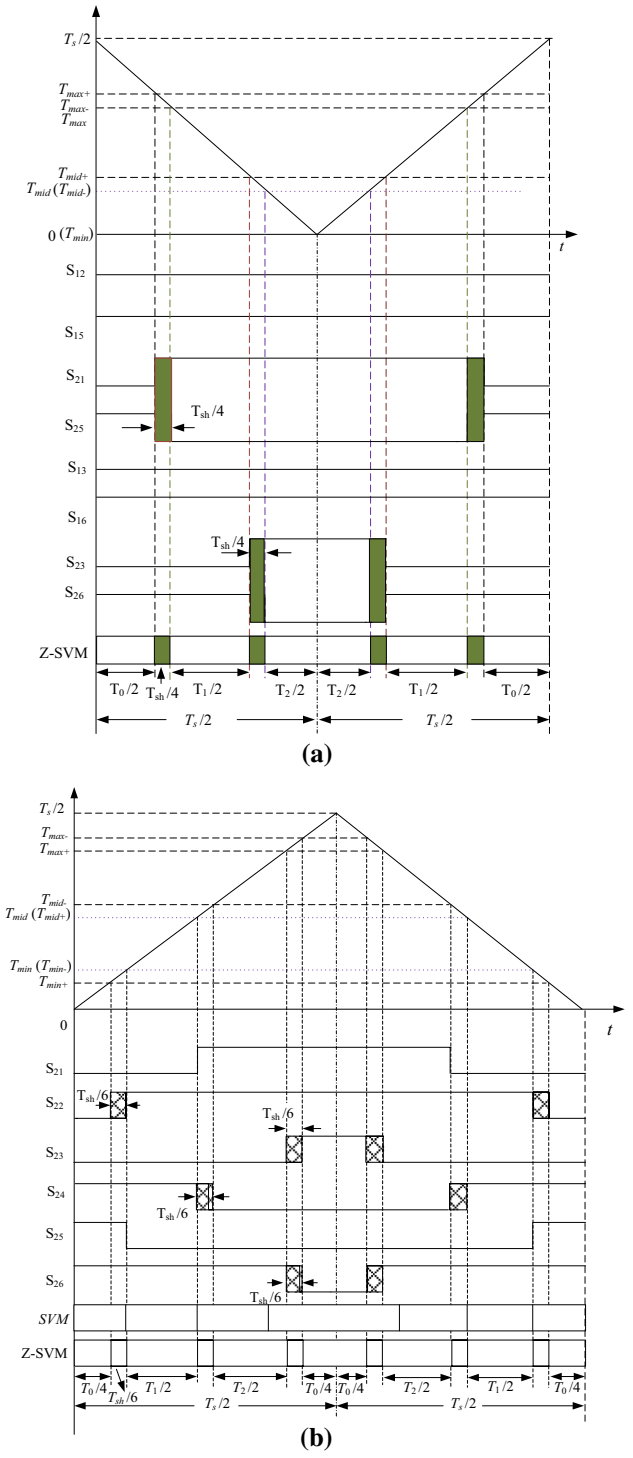

Fig. 9 Drive signals of the power switches for two fault-tolerant topologies: **a** drive signals for the two-phase topology; **b** drive signals for the three-phase topology

seen that the THD value can be significantly reduced after fault tolerance, which verifies the feasibility of the two-phase fault-tolerant control.

Table 3 IM simulation parameters

Design	Parameters	Values
Induction motor (IM) (2.2 kW)	Stator resistance (Rs)	1.875 Ω
	Stator inductance (Ls)	0.1982 H
	Rotor resistance (Rr)	1.741 Ω
	Rotor inductance (Lr)	0.1889 H
	Mutual inductance (Lm)	0.1814 H
	Pole pairs (p)	2
	Inertia (J)	0.0109 kg m^2

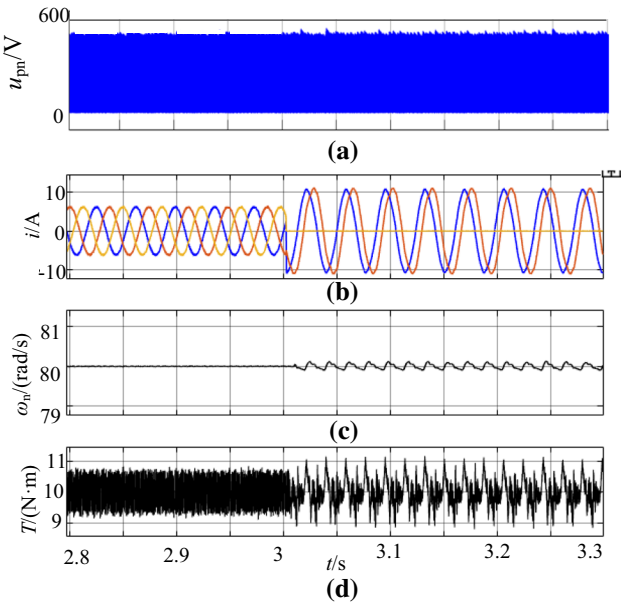

Fig. 10 Simulation waveforms of a two-phase fault-tolerant drive system: **a** DC-link bus voltage; **b** three-phase stator winding current; **c** speed waveform; **d** torque waveform

Through the above analysis, it can be found that both schemes can realize fault-tolerant operation. The two-phase fault-tolerant control (the first fault-tolerant scheme) is very suitable for open-circuit faults of motor windings. The three-phase fault-tolerant control system is suitable for faults of the power switches, where the torque pulsation and the speed pulsation are smaller than those in the two-phase fault-tolerant control.

5 Experimental results

To further verify the performance of the two fault-tolerant schemes, an experimental platform is built, as shown in Fig. 13. It mainly consists of a control board, a sampling regulation circuit and protection circuit board, impedance-source networks, a power board and an induction motor load.

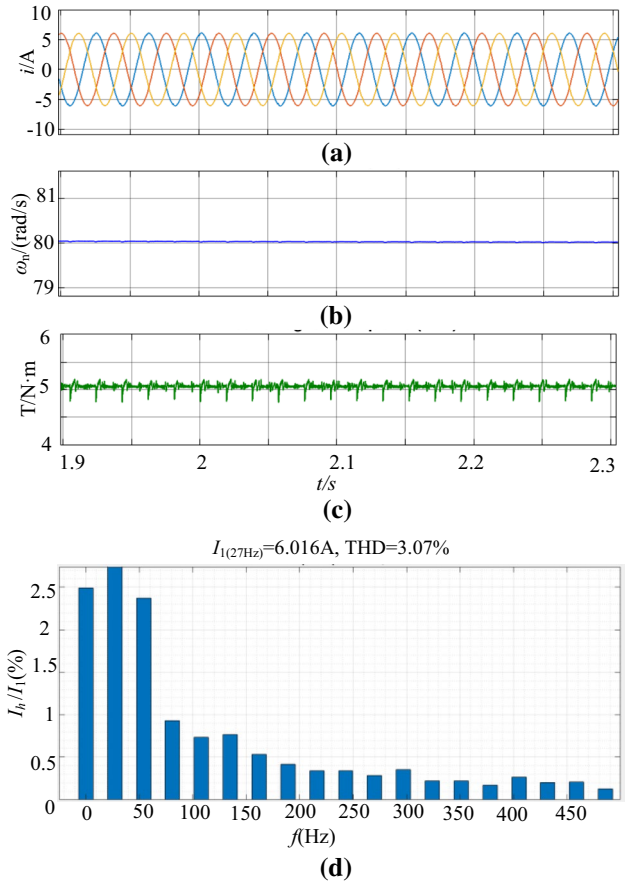

Fig. 11 Simulation waveforms of a three-phase fault-tolerant drive system: **a** three-phase stator winding currents; **b** speed waveform; **c** torque waveform; **d** total harmonic distortion of the one-phase stator winding current

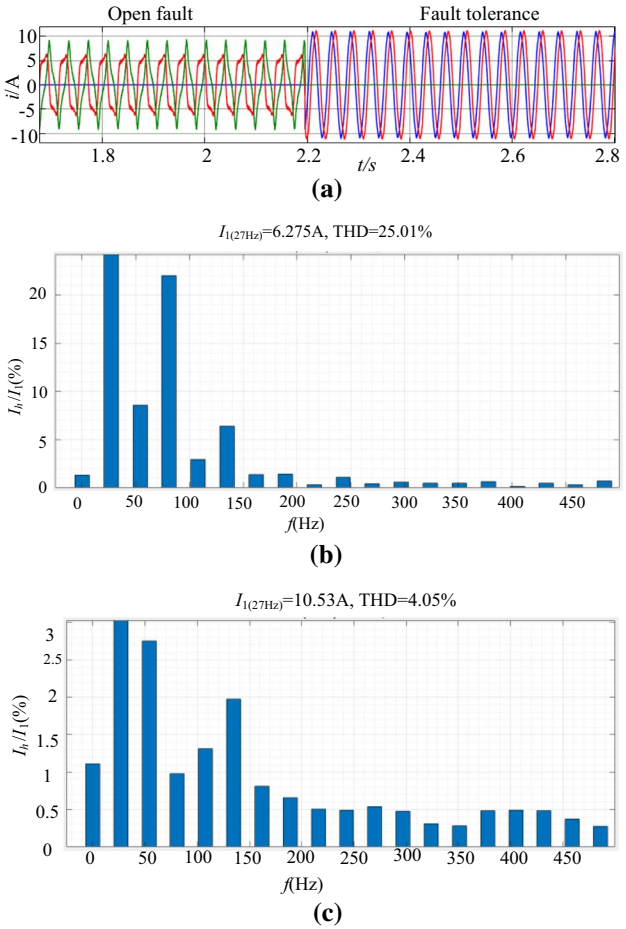

Fig. 12 Stator winding currents and total harmonic distortion (THD) under faulty and fault-tolerant conditions: **a** stator winding currents; **b** THD of one-phase stator winding current under one-phase open-fault condition; **c** THD of one-phase stator winding current under two-phase fault-tolerant condition

In experiments of the drive system, a 1.1 kW traditional asynchronous motor is reconstructed into an open-end winding induction motor. The parameters of the traditional induction motor are shown in Table 4. A photoelectric encoder is adopted to detect the speed. The load is a magnetic powder brake. The DC-link bus voltage of the two inverters is 320 V. The speed of the asynchronous motor is set at 250 rpm. The inductance in the impedance-source network is 1 mH, and the capacitance is 300 μF. In addition, the corresponding experimental results are as follows.

Experimental waveforms of two-phase fault-tolerant control system are shown in Fig. 14. Figure 14a, b shows waveforms of the DC-link bus voltage, one-phase winding voltage and stator winding currents. The amplitude of the two-phase stator winding currents is about 2.1 A, and the current waveforms are sinusoidal. Figure 14c describes the torque. The output speed is 250 rpm, as shown in Fig. 14d. The output speed can still track the given value. From Fig. 14c, d, it can be found that the output torque pulsation and the speed pulsation are large. However, it can continue to work.

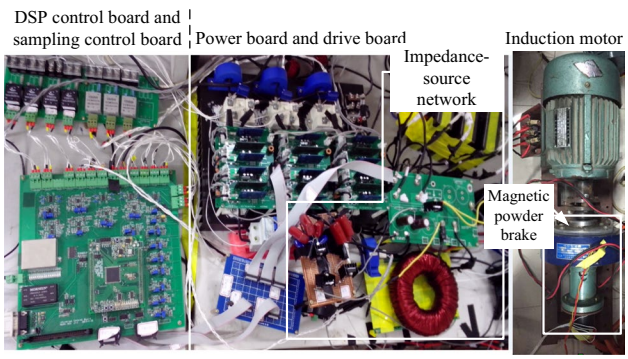

Fig. 13 Experimental prototype

Figure 15 shows experimental waveforms of the three-phase fault-tolerant control system. Figure 15a shows the DC-link bus voltage, winding voltages, and one-phase stator winding current. From Fig. 15b, it can be seen that the

Table 4 Motor specifications

Parameters	Values	Parameters	Values
Rated power	1.1 kW	Connection way	Wye
Rated voltage	380 V	Number of pole-pairs	2
Rated current	2.7 A	Rated speed	1400 r/min

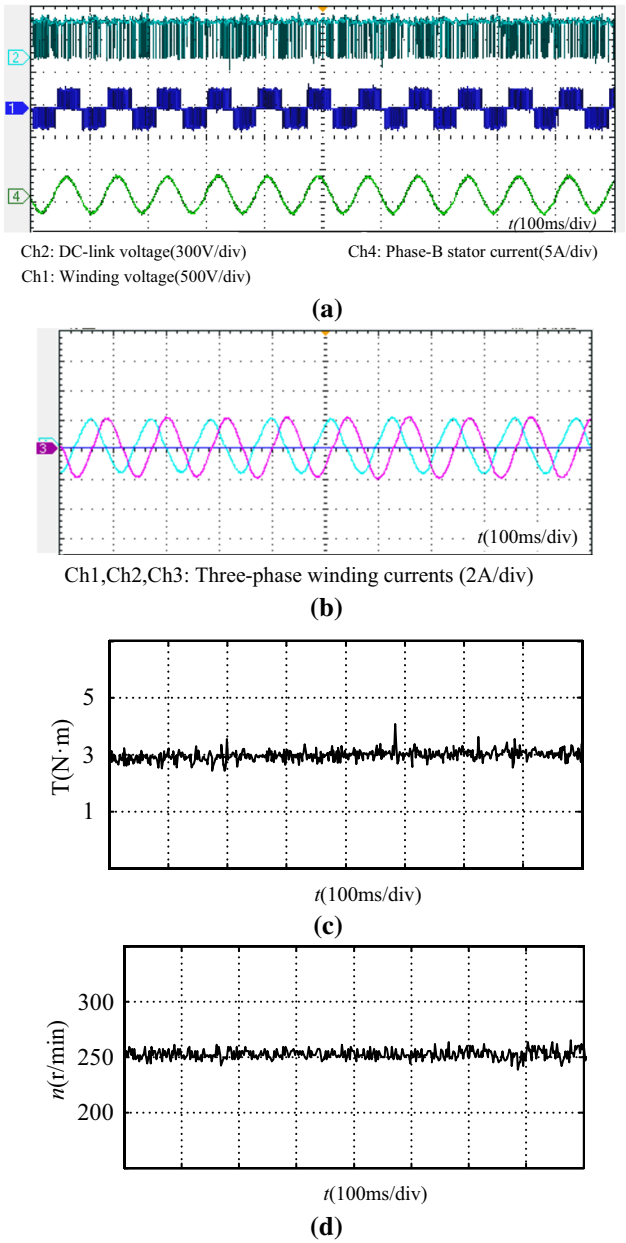

Fig. 14 Experimental waveforms of a two-phase fault-tolerant drive system in the fault-tolerant mode: **a** DC-link bus voltage; **b** three-phase stator winding currents; **c** torque waveform; **d** speed waveform

three-phase stator winding currents are 120° different from each other, and that the current waveforms are sinusoidal with amplitudes of about 2.1 A. The torque waveform is presented in Fig. 15c. From Figs. 14c and 15c, it can be observed that the torque ripple under the three-phase fault-tolerant operation is about 5%, and lower than that under the two-phase fault-tolerant operation. Figure 15d presents a speed waveform. From Fig. 15d, it can be found that the speed can track the given value very well.

When compared with the two-phase fault-tolerant control system, the output torque pulsation and the speed

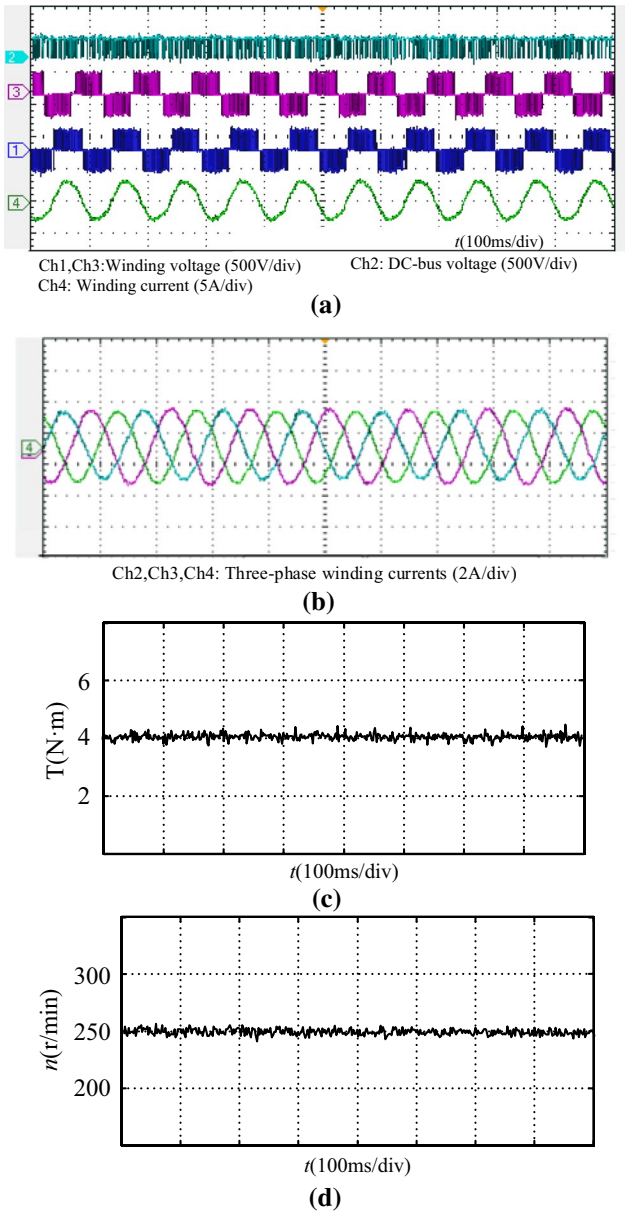

Fig. 15 Experimental waveforms of a three-phase fault-tolerant drive system in the fault-tolerant mode: **a** DC-link bus voltage; **b** three-phase stator winding currents; **c** torque waveform; **d** speed waveform

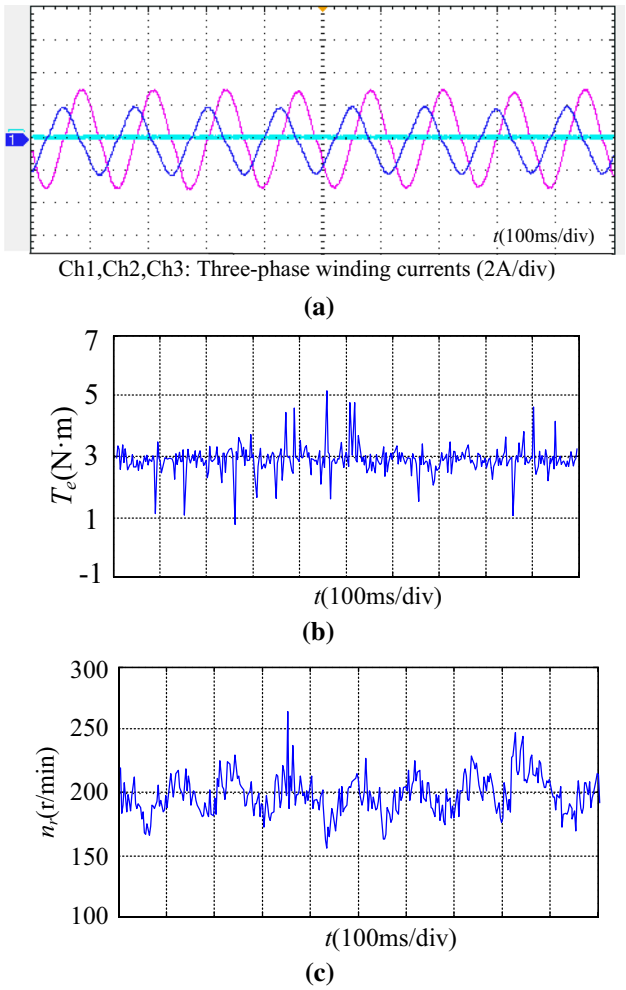

Fig. 16 Experimental waveforms under faulty conditions: **a** three-phase stator winding current; **b** torque waveform; **c** speed waveform

pulsation of three-phase fault-tolerant control system are smaller, its output performance is better, and its implementation is simple. However, the two-phase fault-tolerant drive system is only constructed when an open-circuit fault of the motor winding occurs.

Under the open-winding faulty condition, experimental results are presented in Fig. 16. From Fig. 16, it can be seen that the one-phase winding current is zero, the torque ripple is larger and about 40–50%, and the real speed ripple is larger. Thus, the motor cannot work.

From Figs. 14, 15 and 16, it can be derived that, under fault-tolerant condition, the speed ripple and the torque ripple become smaller, and the drive system can still work well. Therefore, fault-tolerant control of the presented topology is feasible.

6 Conclusion

An open-winding induction motor drive system with boost and fault tolerance is presented in this paper. It is composed of two impedance networks and two traditional three-phase inverters. The drive system is powered by two separate DC supplies and has fault tolerance. A detailed fault-tolerant analysis is addressed. Fault types are mainly open-circuit faults and short-circuit faults. Two fault-tolerant schemes are proposed for open-end winding IM drive systems. In addition, SVPWM methods of the fault-tolerant schemes are presented. Finally, simulation and experimental results of the two fault-tolerant schemes are shown and used to make a comparison. All the presented results confirm that the drive system has fault tolerance and that the fault-tolerant control methods are feasible.

Acknowledgements This work was supported in part by the National Natural Science Foundation of China under Grant 51707085 and Grant 51707086, and by the Natural Science Research Project of Jiangsu Higher Education Institutions of China under Grant 19KJB470020.

References

1. Nguyen, L.V., Tran, H.D., Johnson, T.T.: Virtual prototyping for distributed control of a fault-tolerant modular multilevel inverter for photovoltaics. IEEE Trans. Energy Conversion **29**(4), 841–850 (2014)
2. Fuchs, F. W.: Some diagnosis methods for voltage source inverters in variable speed drives with induction machines—a survey. In: Proceedings of the IEEE Industrial Electronics Society Annual Conference, pp. 1378–1385 (2003).
3. Lahyani, A., Venet, P., Grellet, G., Viverge, P.J.: Failure prediction of electrolytic capacitors during operation of switchmode power supply. IEEE Trans. Power Electron. **13**(6), 1199–1206 (1998)
4. Yu, O. K., Park, N. J., Hyun, D. S.: A novel fault detection scheme for voltage fed PWM inverter. In: Proceedings of the IEEE 32nd Annual Conference on Industrial Electronics, pp 2654–2659 (2006).
5. Pires, F.V., Foito, D., Silva, F.J.: Fault tolerant multilevel topology based on three-Phase H-bridge inverters for open-end winding induction motor drives. IEEE Trans. Energy Conversion **32**(3), 895–902 (2017)
6. Rama Chandra Sekhar, K. and Srinivas, S.: Effect of a CMV elimination PWM on stator current ripple in a dual two-level inverter fed induction motor drive. In: International Symposium on Power Electronics, Electrical Drives, Automation and Motion, pp. 395–400 (2012).
7. Li, C.J., Wang, G.F., Li, F., et al.: Fault-tolerant control for 5L-HNPC inverter-fed induction motor drives with finite control set model predictive control based on hierarchical optimization. J. Power Electron. **19**(4), 989–999 (2019)
8. Nian, H., Zhou, Y., Zeng, H.: Fault-tolerant control technique of permanent magnet synchronous generator based on open winding configuration. Trans. China Electro-tech. Soc. **30**(10), 58–67 (2015)

9. Sekhar, K.R., Srinivas, S.: Torque ripple reduction PWMs for a single DC source powered dual-inverter fed open-end winding induction motor drive. IET Power Electron. **11**(1), 43–51 (2018)
10. Mahato, B., Raushan, R., Jana, K.C.: Modulation and control of multilevel inverter for an open-end winding induction motor with constant voltage levels and harmonics. IET Power Electron. **10**(1), 71–79 (2017)
11. Somasehar, V.T., Srinivas, S., et al.: Pulse width-modulated Switching strategy for the dynamic balancing of zero-sequence current for a dual-inverter fed open-end winding induction motor drive. IET Electr. Power Appl. **1**(4), 591–600 (2007)
12. Somasekhar, V.T., Gopakumar, K., Baiju, M.R., et al.: A multilevel inverter system for an induction motor with open-end windings. IEEE Trans. Ind. Electron. **52**(3), 824–836 (2005)
13. Amerise, A., Mengoni, M., Zarri, L., et al.: Open-end windings induction motor drive with a floating capacitor bridge at variable DC link voltage. IEEE Trans. Ind. Appl. **55**(3), 2741–2749 (2019)
14. Darijevic, M., Jones, M., Levi, E.: An open-end winding four-level five-phase drive. IEEE Trans. Ind. Electron. **63**(1), 538–549 (2016)
15. Rajeevan, P.P., Sivakumar, K., Gopakumar, K., et al.: A nine-level inverter topology for medium voltage induction motor drive with open-end stator winding. IEEE Trans. Ind. Electron. **60**(9), 3627–3636 (2013)
16. Stemmler, H., Guggenbach, P.: Configurations of high-power voltage source inverter drives. Eur. Conf. Power Electron. Appl. **5**, 7–14 (1993)
17. Lakhimsetty, S., Surulivel, N., Somasekhar, V.: Improvised SVPWM strategies for an enhanced performance for a four-level open-end winding induction motor drive. IEEE Trans. Ind. Electron. **64**(4), 2750–2759 (2017)
18. Reddy, B.V., Somasekhar, V.T.: An SVPWM scheme for the suppression of zero-sequence current in a four-level open-end winding induction motor drive with nestedrectifier-inverter. IEEE Trans. Ind. Electron. **63**(5), 2803–2812 (2016)
19. Kunisetti, V., Kumar, P., Kumar, T.V.: Predictive torque control of open-end winding induction motor drive fed with multilevel inversion using two two-level inverters. IET Electric Power Appl. **12**(1), 54–62 (2018)
20. Srinivasan, P., Narasimharaju, B.L., Rikanth, N.V.: Space-vector pulse width modulation scheme for open-end winding induction motor drive configuration. IET Power Electron. **8**(7), 1083–1094 (2015)
21. Zhao, W.X., Zhao, P., Xu, D.Z., et al.: Hybrid modulation fault-tolerant control of open-end windings linear vernier permanent-magnet motor with floating capacitor inverter. IEEE Trans. Power Electron. **34**(3), 2563–2572 (2019)
22. Siwakoti, Y.P., Peng, F.Z., Blaabjerg, F., et al.: Impedance-source networks for electric power conversion Part I: A topological review. IEEE Trans. Power Electron. **30**(2), 699–716 (2015)
23. Peng, F.Z., Joseph, A., Wang, J., et al.: Z-source inverter for motor drives. IEEE Trans. Power Electron. **20**(4), 857–863 (2005)
24. Ayad, A., Hanafiah, S., Kennel, R.: A comparison of quasi-z-source inverter and traditional two-stage inverter for photovoltaic application. In: International Exhibition and Conference for Power Electronics, Intelligent Motion, Renewable Energy and Energy Management (PCIM Europe), pp. 1580–1587 (2015).
25. Liu, Y.S., Ge, B.M., Abu-Rub, H., Peng, F.Z.: Overview of space vector modulations for three-phase Z-source/quasi-Z-source inverters. IEEE Trans. Power Electron. **29**(4), 2098–2108 (2014)
26. Baranwal, R., Basu, K., Mohan, N.: Dual two level inverter carrier SVPWM with zero common mode voltage. In: IEEE International Conference on Power Electronics, Drives and Energy Systems (PEDES), pp 1–6 (2012).
27. Lu, B., Sharma, S.K.: A literature review of IGBT fault diagnostic and protection methods for power inverters. IEEE Trans. Ind. Appl. **45**(5), 1770–1777 (2009)
28. Mendes, A. M. S. and Marques Cardoso, A. J.: Voltage source inverter fault diagnosis in variable speed ac drives, by the average current Park's vector approach. In: IEEE International Electric Machines and Drives Conference, pp 704–706, (1999).

Chunjie Li received her B.S. and M.S. degrees in Electrical Engineering from the Shandong University of Science and Technology, Qingdao, China, in 2008 and 2011, respectively. She received her Ph.D. degree in Power Electronics and Electrical Drives from the Nanjing University of Aeronautics and Astronautics, Nanjing, China, in 2016. In 2016, she joined the faculty of the College of Electrical Engineering and Automation, Jiangsu Normal University, Xuzhou, China, where she is presently working as a Lecturer. Her current research interests include power electronics and the control of electrical machine systems.

Guifeng Wang received his B.S. and M.S. degrees from School of Information and Electrical Engineering at the China University of Mining and Technology, Xuzhou, China, in 2004 and 2007, respectively. He received his Ph.D. degree in Power Electronics and Electrical Drive from Shanghai Jiao Tong University, Shanghai, China. He is presently working as a Senior Engineer in the College of Electrical Engineering and Automation, Jiangsu Normal University, Xuzhou, China. His current research interests include power electronic converters for electrical drives and power quality.

Hongmei Li received her B.S. degree in Electrical Engineering from the Shandong University of Science and Technology, Qingdao, China, in 1995; and her Ph.D. degree in Electrical Engineering from Southeast University, Nanjing, China, in 2015. She is a Member of the China Electrical Engineering Society. Her current research interests include the stability and control of power systems and new energy.

Fei Li received his B.S. degree from the China University of Mining and Technology, Xuzhou, China, in 2005; his M.S. degree from the University of Duisburg-Essen, Duisburg and Essen, Germany, in 2009; and his Ph.D. degree from the China University of Mining and Technology, in 2017. His current research interests include power electronics converters and power quality.

Zhenglong Xia received his B.S. and Ph.D. degrees from the School of Information and Electrical Engineering, China University of Mining and Technology, Xuzhou, China, in 2005 and 2014, respectively. In 2014, he became a Lecturer in the school of Electrical Engineering and Automation, Jiangsu Normal University, Xuzhou, China. He has published more than 20 research papers in journals. His current research interests include the reactive compensation of power systems, fault diagnosis, distributed parallel processing and neural networks.

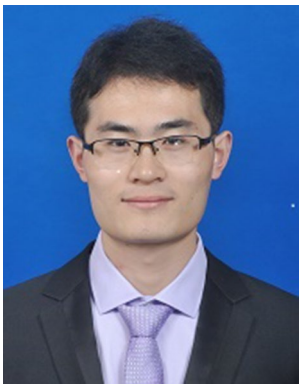

Zhan Liu received his Ph.D. degree in Electrical Engineering and Automation from the China University of Mining and Technology, Xuzhou, China, in 2016. He is presently working as a Faculty Member in the School of Electrical Engineering and Automation, Jiangsu Normal University, Xuzhou, China. His current research interests include power electronics, modern control theory and multilevel converters.